Energies of molecular structures in ^{12}C,^{16}O,^{20}Ne,^{24}Mg, and ^{32}S

G. Royer, G. Ramasamy, and P. Eudes
Laboratoire Subatech, UMR: IN2P3/CNRS Université Ecole des Mines, Nantes 44, France
(Received 15 July 2015; published 16 November 2015)

The energies of the ^{12}C,^{16}O,^{20}Ne,^{24}Mg, and ^{32}S $4n$ nuclei have been determined within a generalized liquid drop model and assuming different planar and three-dimensional shapes of the α molecules: linear chain, triangle, square, tetrahedron, pentagon, trigonal bipyramid, square pyramid, hexagon, octahedron, octagon, and cube. The potential barriers governing the entrance and decay channels via α absorption or emission as well as more symmetric binary and ternary reactions have been compared. The rms radii of the linear chains differ from the experimental rms radii of the ground states. The binding energies of the three-dimensional shapes at the contact point are higher than the ones of the planar configurations. The α particle plus A-4 daughter configuration leads always to the lowest potential barrier. The binding energy can be reproduced within the sum of the binding energy of n α particles plus the number of bonds multiplied by 2.4 MeV or by the sum of the binding energies of one α particle and the daughter nucleus plus the Coulomb energy and the proximity energy.

DOI: 10.1103/PhysRevC.92.054308 PACS number(s): 21.60.Gx, 26.20.Fj, 25.60.Pj, 23.60.+e

I. INTRODUCTION

α particles play a main role in the nucleosynthesis of ^{12}C,^{16}O, and heavier elements and α-particle models have been developed [1–4]. Cluster-type states coexist with the mean-field-type states in these $4n$ nuclei [5,6].

Theoretically, in ^{12}C the ground-state wave function contains a large amount of the 3α cluster wave function. In ^{16}O some excited states are due to the mean-field-type excitation mode while others are dominantly of the cluster structure of $\alpha + {}^{12}$C [5]. For ^{16}O, recent *ab initio* lattice calculations using effective field theory lead for the ground state to a tetrahedral configuration of α clusters and for the first excited spin-0 state and first spin-2 state to a square configuration, in good agreement with the empirical energy spectrum and with the electromagnetic properties and transition rates [7]. Within an algebraic cluster model, a comparison with the experimental values of the energy of the low-lying spectrum and electromagnetic transitions have also provided strong evidence for tetrahedral symmetry in ^{16}O [8]. Using a cranked Skyrme Hartree-Fock method the existence in ^{16}O of a region of angular momentum (13–18 $\hbar$) where the linear chain configuration is stabilized has been demonstrated [9]. It has also been shown [10] that the high fragmentation into several peaks of the giant dipole resonance spectra of ^{12}C and ^{16}O is due to the different α structures of these nuclei. In connection with the excited 0_2^+ Hoyle state of ^{12}C ($E^* = 7.65$ MeV) and possible excited Hoyle state of ^{16}O ($0_6^+, E^* = 15.1$ MeV), the α condensate character of the α linear chain has been proposed after comparing a large number of Brink functions with Tohsaki-Horiuchi-Schuck-Röpke wave functions [11,12]. In ^{20}Ne the ground band states contain the $\alpha + {}^{16}$O component at most 70% [5]. Within a three-dimensional cranked Skyrme Hartree-Fock method a stable state in ^{40}Ca with a torus configuration has been obtained at 60 $\hbar$ and with an excitation energy of about 170 MeV [13].

Experimentally, in ^{12}C, a new high spin 5^- state at 22.4 MeV has been measured recently [14]. It fits very well the ground-state rotational band of an oblate equilateral triangular spinning top with a D_{3h} symmetry characterized by the sequence $0^+,2^+,3^-,4^\pm,5^-$. For the 0_2^+ excited Hoyle state of ^{12}C an upper limit of 0.2% on the direct 3α decay has been obtained [15]. For the excited rotational band of ^{16}O, an $\alpha + {}^{12}$C resonant cluster structure has also been observed [16] as well as a 4α linear chain [17,18]. In the nucleus ^{24}Mg in the range of 14–16 $\hbar$ analysis of experimental data suggests that extremely prolate linear α chains are populated [19]. Possible signatures of α clustering in light nuclei from relativistic collisions have been suggested [20]. An α-^{208}Pb structure has also been observed in ^{212}Po [21].

In a previous work [22] the L-dependent energies and potential barriers governing the evolution of the $^{8}\text{Be} \leftrightarrow {}^{4}\text{He} + {}^{4}\text{He}$ and $^{12}\text{C} \leftrightarrow {}^{8}\text{Be} + {}^{4}\text{He}$ systems and the $^{12}\text{C} \leftrightarrow {}^{4}\text{He} + {}^{4}\text{He} + {}^{4}\text{He}$ oblate triangular and prolate longitudinal configurations have been determined in the framework of a generalized liquid drop model (GLDM) and of binary and ternary quasimolecular shapes. The purpose of the present work is to apply the same approach to study the ^{12}C,^{16}O,^{20}Ne,^{24}Mg, and ^{32}S $4n$ nuclei assuming different planar and three-dimensional α molecules: linear chain, triangle, square, tetrahedron, pentagon, trigonal bipyramid, square pyramid, hexagon, octahedron, octagon, and cube (see Fig. 1). Within the α cluster model approach this study considers separated α particles starting from their contact point since it is extremely difficult mathematically to describe the strongly deformed one-body shapes appearing just before the birth of several α particles and the transition from one quasispherical nucleus. Since the coexistence of cluster states and mean-field-type states in ^{12}C,^{16}O,^{20}Ne,^{24}Mg, and ^{32}S is well established, ground states and entrance and decay channels of these nuclei have been also determined assuming spherical shapes and, then, their potential energies have been calculated continuously from one spherical nucleus to two or three spherical aligned nuclei [23,24] using generalized elliptic lemniscatoids.

II. POTENTIAL ENERGY

To determine the energy of these light nuclear systems the GLDM has been used once again. It has previously

FIG. 1. Planar and three-dimensional molecular shapes.

been defined to calculate in an unified way and without new adjustment of parameters the fusion [25–27] and binary [28] and ternary [23,24] fission barriers, the barriers against α [29] and cluster emissions [30].

The GLDM energy is the sum of the volume, surface, Coulomb, and nuclear proximity energies. This proximity energy term is still often neglected because it appears only where there are deep necks or crevices in strongly deformed compact nuclear one-body shapes or between two separated spherical or ellipsoidal nuclei. It does not contribute to the mass formula or to the energy of elongated shapes with very shallow necks. In contrast it plays a main role to reproduce the fusion barriers beyond the pure unrealistic Coulomb peak, the fission barriers through quasimolecular shapes, and the energy of nuclear molecules. For example, the proximity energy reaches -9.4 MeV between two α particles at the contact point. The GLDM and particularly the proximity energy term are detailed in Refs. [22,25].

This macroscopic approach is complementary to the microscopic mean-field studies which focus on the variations appearing in the nuclear densities of one-body nuclear systems and do not consider explicitly separated multibody shapes and the usual clearly defined molecular structures.

III. ^{12}C NUCLEUS

Without assuming α clustering, calculations using antisymmetrized molecular dynamics and fermionic molecular dynamics have led for the shapes of the different states of ^{12}C to triangular α molecules with different angles allowing the reproduction of the low-lying spectrum of ^{12}C [31–33]. Using effective field theory and Monte Carlo *ab initio* lattice calculations it has been found that the ^{12}C ground state and the first excited 2_1^+ state have a compact triangular configuration while the Hoyle state and the second excited 2_2^+ state have a "bent-arm" or obtuse triangular configuration of α clusters [34]. These theoretical predictions are strengthened by the recent observation of a new high spin 5^- state at 22.4 MeV compatible with a ground-state rotational band of an oblate equilateral triangular spinning top with a D_{3h} symmetry characterized by the sequence $0^+,2^+,3^-,4^\pm,5^-$, but the Hoyle state is then interpreted as the band head of the A-symmetric stretching vibration or breathing mode of the triangular configuration [14]. Therefore the structure of the Hoyle state is still controversial [15].

To study these oblate ternary configurations within the GLDM, three α particles are placed at the top on an isosceles triangle and later on they separate and move away from each other while keeping the same triangular configuration characterized by the angle θ (see Fig. 2). At the contact point the energy of the equilateral triangular shape is lower than the energy of the linear chain of three α ($\theta = 180^\circ$), the energy difference being 7.36 MeV. This is also in favor of

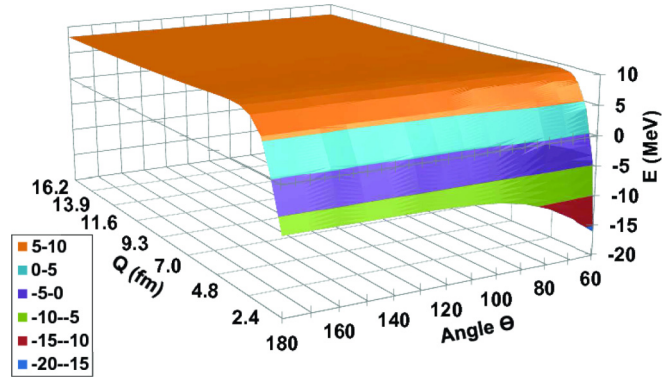

FIG. 2. (Color online) Potential energy of an isosceles triangular α molecule as a function of the angle θ (deg.) and the root-mean-square radius Q.

an equilateral triangular configuration for the ground state and a more aligned chain for the Hoyle state (the energy is almost constant between 120° and 180°). For the ground state the experimental rms charge radius is $\langle r^2\rangle^{1/2} = 2.47$ fm. With the radius formula of the GLDM, at the contact point the rms radius is 2.43 fm for a triangular molecule and 3.16 fm for a linear chain. Furthermore experimentally the electric quadrupole moment is negative, which is inconsistent with three aligned α particles for the ground-state shape [22].

IV. ^{16}O NUCLEUS

Since for the ground state a tetrahedral configuration of α clusters is predicted [7,8] and for the first excited spin-0 state a square configuration [7] it is worthwhile to investigate these shapes within a GLDM. In Fig. 3 the energies of these two configurations are compared. At the contact point between the four spherical α particles the rms radius is 2.54 fm for a tetrahedron, 2.83 fm for a square (which is less compact than a tetrahedron), and 4.15 fm for a linear chain. Experimentally the rms charge radius of the ground state is $\langle r^2\rangle^{1/2} = 2.70$ fm which seems to exclude a linear chain configuration for the ground state. The binding energy

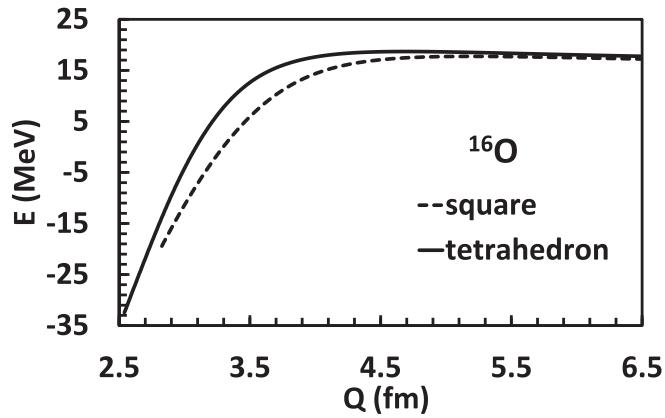

FIG. 3. Potential energies of square and tetrahedral configurations from the contact point as a function of the rms radius.

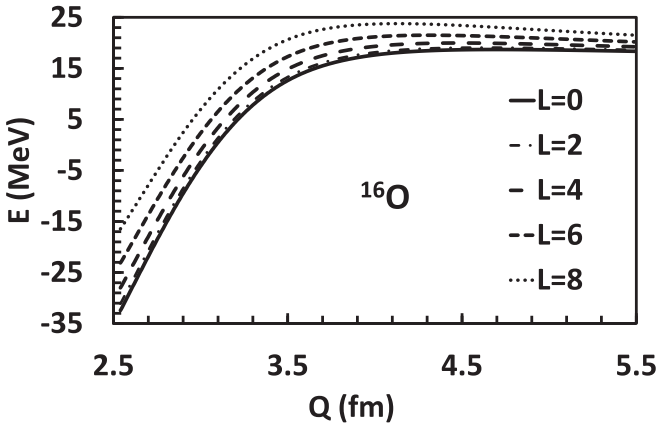

FIG. 4. Potential energy of the α tetrahedron as a function of the angular momentum (in $\hbar$ unit) and rms radius.

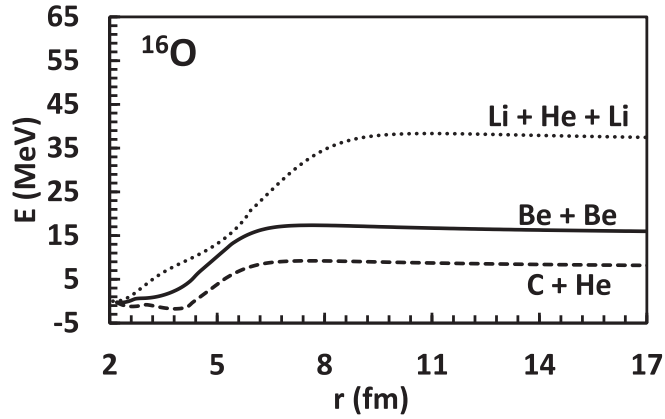

FIG. 6. Potential barriers governing the $^{12}C + {}^{4}He$, $^{8}Be + {}^{8}Be$, and linear $^{6}Li + {}^{4}He + {}^{6}Li$ nuclear systems versus the distance between the mass centers (at $L = 0$).

is higher for the tetrahedral configuration than for the square shape since for these molecular configurations the proximity energy plays the main role and there are six bonds for the tetrahedron and only four for the square. On the contrary, the Coulomb repulsion (which is small) is lower for the square at the contact point. The energy difference is 13.7 MeV close to $Q_{4\alpha}$ (14.4 MeV), the energy of the 0^+_6 state (15.1 MeV), and 14.03 MeV the energy of a 0^+ state. The electric quadrupole moment of the square shape is $Q_0 = -49.2\ e\,\mathrm{fm}^2$.

The L-dependent energies of the tetrahedron and square are shown in Figs. 4 and 5. For the tetrahedral shape the relative energies at the contact point are, respectively, 0, 1.3, 4.4, 9.3, and 16 MeV for $L = 0$, 2, 4, 6, and 8 $\hbar$ and for the square 0, 1.1, 3.5, 7.4, and 12.6 MeV for $L = 0$, 2, 4, 6 and 8 $\hbar$.

Since the ground state is also seen as double closed shell wave function and several low-lying excited states are described within the $^{12}C + {}^{4}He$ cluster model [5] the potential energies of the $^{12}C + {}^{4}He$, $^{8}Be + {}^{8}Be$, and linear $^{6}Li + {}^{4}He + {}^{6}Li$ systems have been determined assuming a spherical shape for the compound nucleus and each cluster (see Fig. 6). The different threshold energies are 7.16 MeV for $Q_{^{4}He+^{12}C}$, 14.44 for $Q_{4\alpha}$, 14.62 for $Q_{^{8}Be+^{8}Be}$, and 35.34 for $Q_{^{6}Li+^{4}He+^{6}Li}$. The top of the barrier corresponds to separated nuclei maintained in unstable equilibrium by the balance between the repulsive Coulomb forces and the attractive nuclear proximity forces. In the $^{12}C + {}^{4}He$ channel, quasimolecular one-body shapes have almost the same energy as the spherical nucleus. Experimentally the breakup of ^{16}O (at 4.5 GeV/nucleon) into two α and a ^{8}Be has been observed using nuclear emulsions [35].

V. ^{20}Ne NUCLEUS

For ^{20}Ne the pentagon, trigonal bipyramid, and square pyramid shapes have been investigated with the GLDM. The energies of these three configurations are compared in Fig. 7. At the contact point the rms radius is 2.76 fm for a trigonal bipyramid, 2.79 fm for a square pyramid, and 3.29 fm for a pentagon. The experimental rms charge radius is $\langle r^2\rangle^{1/2} = 3.01$ fm far below the rms radius of a linear chain. The binding energy is higher for the trigonal bipyramid than for the square pyramid and the pentagon. The proximity energy at the contact point between two α increases the binding energy

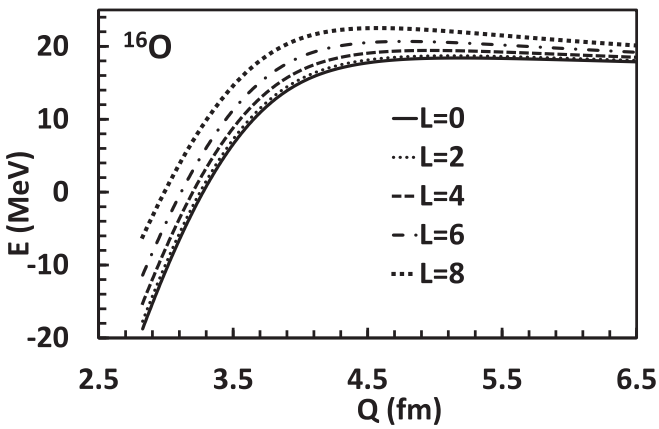

FIG. 5. Potential energy of the α square as a function of the angular momentum (in $\hbar$ unit) and rms radius.

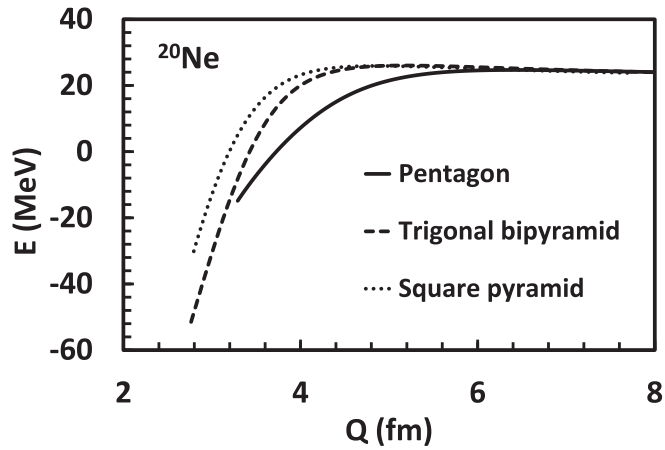

FIG. 7. Potential energies of a pentagon, trigonal bipyramid, and square pyramid from the contact point as a function of the rms radius.

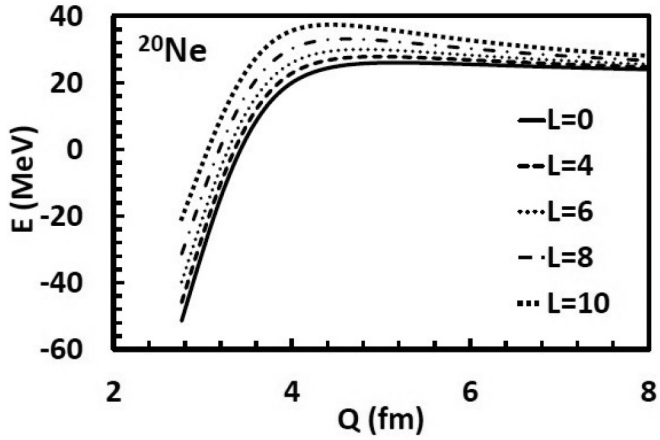

FIG. 8. Potential energy of the α bipyramid as a function of the angular momentum (in $\hbar$ unit) and rms radius.

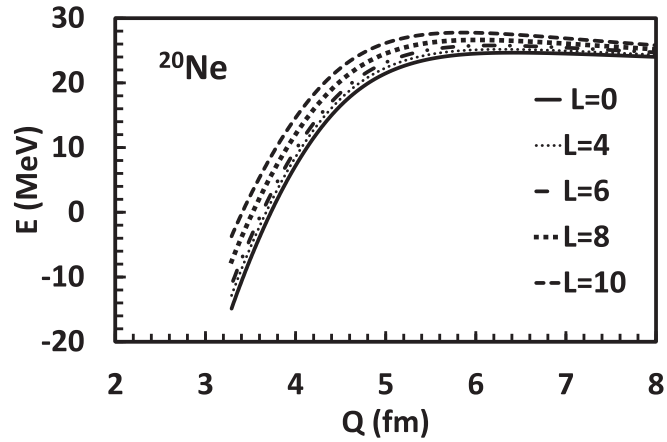

FIG. 10. Potential energy of the α pentagon as a function of the angular momentum (in $\hbar$ unit) and rms radius.

and acts five times in the pentagon, eight in the square pyramid, and nine times for the trigonal bipyramid. The Coulomb energy varies in the other sense. The energy difference between the trigonal bipyramid and the square pyramid is 21.3 MeV and 15.3 between the square pyramid and the pentagon at the contact point, while $Q_{5\alpha} = 19.17$ MeV. The electric quadrupole moment of the trigonal bipyramid, square pyramid, and pentagon are, respectively, 41.3, -29.7, and -89.6 e fm^2.

The L-dependent energies of the trigonal bipyramid, square pyramid, and pentagon configurations are shown in Figs. 8, 9, and 10. For the trigonal bipyramid the relative energies to the ground state at the contact point are respectively 0, 1.7, 5.6, 11.7 and 20.1 MeV for $L = 0$, 2, 4, 6, and 8 $\hbar$; for the square pyramid it is 0, 1.0, 3.2, 6.8, and 11.7 MeV for $L = 0$, 2, 4, 6, and 8 $\hbar$. For the pentagon the values are 0, 0.6, 2.0, 4.3, and 7.3 MeV for $L = 0$, 2, 4, 6, and 8 $\hbar$. Experimentally the energies of the 2_0^+ and 4_0^+ states are, respectively, 1.63 and 4.25 MeV.

In ^{20}Ne the ground band states contain the ^{16}O + ^{4}He component at most 70% [5]. The potential energies of the ^{16}O + ^{4}He, ^{12}C + ^{8}Be, ^{10}B + ^{10}B, and linear ^{8}Be + ^{4}He + ^{8}Be systems have been calculated assuming spherical shapes for all the nuclei (see Fig. 11). The different threshold energies are 4.73 MeV for $Q_{^{16}O+^4He}$, 11.98 for $Q_{^8Be+^{12}C}$, 19.35 for $Q_{^8Be+^4He+^8Be}$, and 31.14 MeV for $Q_{^{10}B+^{10}B}$. In the ^{16}O + ^{4}He channel, quasimolecular one-body shapes have almost the same energy as the spherical nucleus and the minimum has a cluster structure corresponding roughly to the two ^{4}He and ^{16}O nuclei in contact. Experimentally the breakup of ^{20}Ne (at 3.65 GeV/nucleon) with the emission of five α (partially as ^{8}Be) has been registered in nuclear emulsions [35].

VI. ^{24}Mg NUCLEUS

For ^{24}Mg the energies of the hexagonal and octahedral α molecules are indicated in Fig. 12. For the ground state the experimental rms charge radius is $\langle r^2 \rangle^{1/2} = 3.06$ fm. At the contact point the rms radius is 3.79 fm for a hexagon, and 2.85 fm for an octahedron, which seems to exclude the planar configuration and the linear chain as possible ground-state shapes.

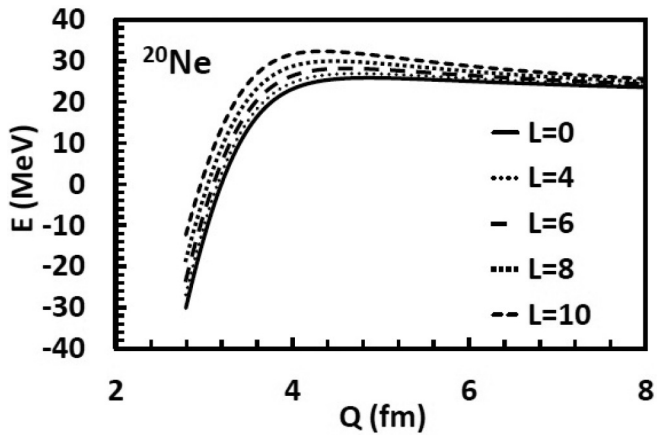

FIG. 9. Potential energy of the α square pyramid as a function of the angular momentum (in $\hbar$ unit) and rms radius.

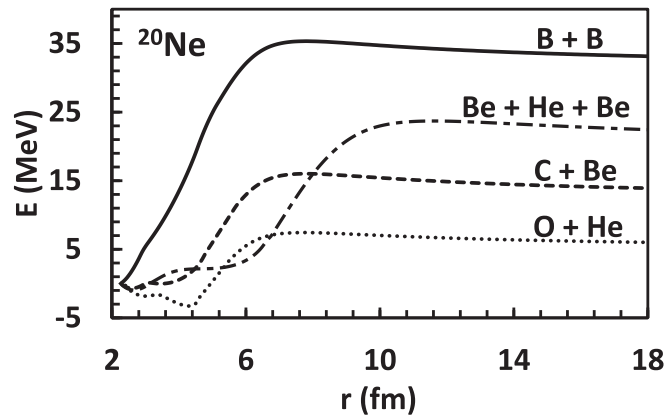

FIG. 11. Potential barriers governing the ^{16}O + ^{4}He, ^{12}C + ^{8}Be, ^{10}B + ^{10}B, and linear ^{8}Be + ^{4}He + ^{8}Be reactions versus the distance between the mass centers (at $L = 0$).

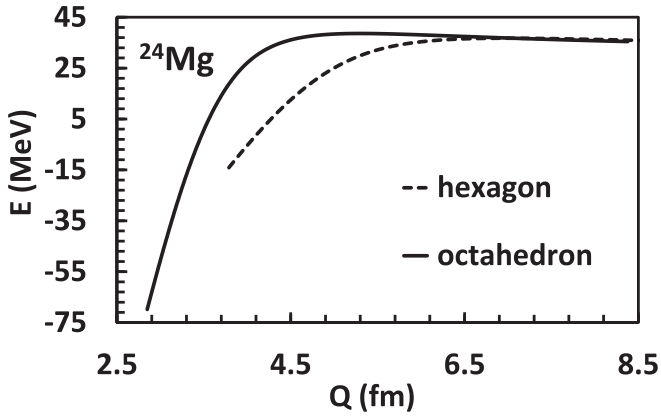

FIG. 12. Potential energies of a hexagon and an octahedron from the contact point as a function of the rms radius.

More generally the rms radii given by the GLDM at the contact point of the equilateral triangle, tetrahedron, trigonal bipyramid or square pyramid, and octahedron are slightly lower than the experimental rms radii of the ground states of the ^{12}C,^{16}O,^{20}Ne, and ^{24}Mg nuclei. Keeping in mind that the formula used in the GLDM leads to a low value of the nuclear radius, one may consider that the contact point of these three-dimensional shapes corresponds roughly to the ground state (within the cluster picture) and then to the minimum of the potential energy even though real minima do not appear on the curves, since the very distorted one-body shapes corresponding to nascent several fragments still linked together are not considered.

For ^{24}Mg the binding energy is higher for the octahedral configuration than for the hexagonal shape since there are 12 bonds for the octahedron and only 6 for the hexagon. The electric quadrupole moment of the hexagon is $-149.7\ e\,\mathrm{fm}^2$.

The potential energies of the $^{16}\mathrm{O} + {}^{8}\mathrm{Be}$, $^{12}\mathrm{C} + {}^{12}\mathrm{C}$, $^{8}\mathrm{Be} + {}^{8}\mathrm{Be} + {}^{8}\mathrm{Be}$, and $^{10}\mathrm{B} + {}^{4}\mathrm{He} + {}^{10}\mathrm{B}$ systems are displayed in Fig. 13. The different Q values are 9.32 MeV for $Q_{^{4}\mathrm{He}+^{20}\mathrm{Ne}}$, 13.93 for $Q_{^{12}\mathrm{C}+^{12}\mathrm{C}}$, 14.14 for $Q_{^{8}\mathrm{Be}+^{16}\mathrm{O}}$, 28.48 for $Q_{6\alpha}$, 28.76 for $Q_{^{8}\mathrm{Be}+^{8}\mathrm{Be}+^{8}\mathrm{Be}}$, and 40.46 for $Q_{^{10}\mathrm{B}+^{4}\mathrm{He}+^{10}\mathrm{B}}$.

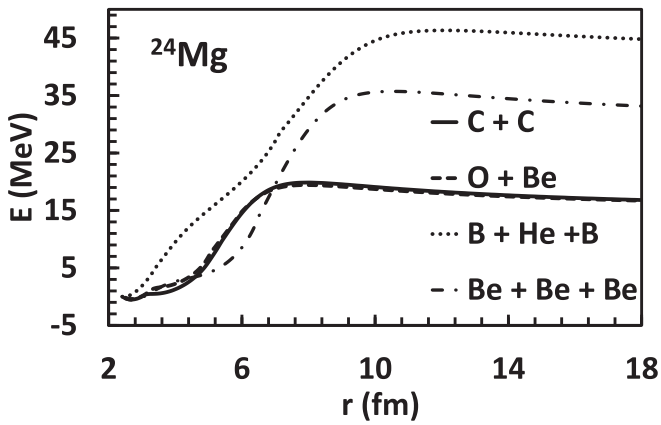

FIG. 13. Potential barriers governing the $^{16}\mathrm{O} + {}^{8}\mathrm{Be}$, $^{12}\mathrm{C} + {}^{12}\mathrm{C}$, linear $^{8}\mathrm{Be} + {}^{8}\mathrm{Be} + {}^{8}\mathrm{Be}$, and $^{10}\mathrm{B} + {}^{4}\mathrm{He} + {}^{10}\mathrm{B}$ reactions versus the distance between the mass centers.

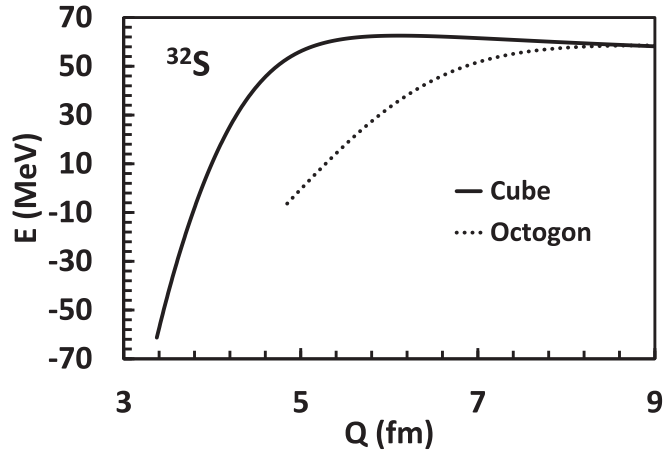

FIG. 14. Potential energies of an octagonal molecule and a cubic molecule from the contact point as a function of the rms radius.

VII. ^{32}S NUCLEUS

For ^{32}S the octagonal and cubic α molecules have been studied. Their energies are displayed in Fig. 14. The experimental rms charge radius of the ground state is $\langle r^2\rangle^{1/2} = 3.26$ fm. At the contact point the rms radius is 4.85 fm for an octagon, and 3.37 fm for a cube, which excludes the planar and linear configurations. The binding energy is higher for the cubic molecule than for the octagonal shape since there are 12 bonds for the cube and only 8 for the octagon. The electric quadrupole moment of the octogon is $-345.3\ e\,\mathrm{fm}^2$.

The potential energies of the $^{28}\mathrm{Si} + {}^{4}\mathrm{He}$, $^{24}\mathrm{Mg} + {}^{8}\mathrm{Be}$, $^{20}\mathrm{Ne} + {}^{12}\mathrm{C}$, and $^{16}\mathrm{O} + {}^{16}\mathrm{O}$ systems are displayed in Fig. 15. The different threshold energies are 6.95 MeV for $Q_{^{4}\mathrm{He}+^{28}\mathrm{Si}}$, 16.54 for $Q_{^{16}\mathrm{O}+^{16}\mathrm{O}}$, 17.02 for $Q_{^{8}\mathrm{Be}+^{24}\mathrm{Mg}}$, 18.97 for $Q_{^{12}\mathrm{C}+^{20}\mathrm{Ne}}$, 30.96 for $Q_{^{12}\mathrm{C}+^{8}\mathrm{Be}+^{12}\mathrm{C}}$, 34.17 for $Q_{^{14}\mathrm{N}+^{4}\mathrm{He}+^{14}\mathrm{N}}$, and 45.42 for $Q_{8\alpha}$. The energy of the $^{28}\mathrm{Si} + {}^{4}\mathrm{He}$ one-body nucleus is relatively constant until the spherical nucleus, allowing the cohabitation of different quasimolecular shapes. The superdeformed band contains the $^{16}\mathrm{O} + {}^{16}\mathrm{O}$ component by about 44% [5].

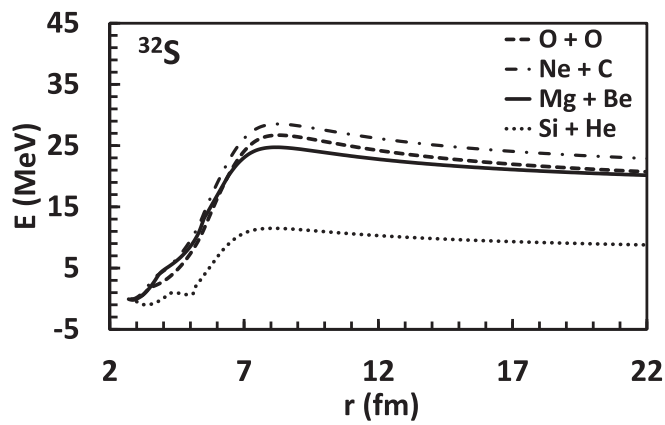

FIG. 15. Potential barriers governing the $^{28}\mathrm{Si} + {}^{4}\mathrm{He}$, $^{24}\mathrm{Mg} + {}^{8}\mathrm{Be}$, $^{20}\mathrm{Ne} + {}^{12}\mathrm{C}$, and $^{16}\mathrm{O} + {}^{16}\mathrm{O}$ reactions versus the distance between the mass centers.

VIII. BINDING ENERGY

From the experimental binding energies it is known that they can be reproduced within the molecular structures by the sum of the binding energy of n α plus the number of bonds multiplied by around 2.4 MeV.

$$\begin{aligned} B(^{12}\mathrm{C}) &= 3 \times B(\alpha) + 3(\mathrm{bonds}) \times 2.42\ \mathrm{MeV}, \\ B(^{16}\mathrm{O}) &= 4 \times B(\alpha) + 6(\mathrm{bonds}) \times 2.41\ \mathrm{MeV}, \\ B(^{20}\mathrm{Ne}) &= 5 \times B(\alpha) + 8(\mathrm{bonds}) \times 2.40\ \mathrm{MeV}, \\ B(^{24}\mathrm{Mg}) &= 6 \times B(\alpha) + 12(\mathrm{bonds}) \times 2.37\ \mathrm{MeV}. \end{aligned} \tag{1}$$

From the GLDM it is difficult to explain this value of 2.4 MeV per bond since it does not correspond to the sum of the proximity energy and the mean Coulomb repulsion by bond.

The binding energy of these nuclei may also be calculated within the GLDM and a core $+\alpha$ cluster model since the energy corresponds to the sum of the binding energies of one α and one daughter nucleus plus roughly the Coulomb energy and the proximity energy between the two nuclei.

$$\begin{aligned} B(^{12}\mathrm{C}) &= B(^{8}\mathrm{Be}) + B(\alpha) + 7.37\ \mathrm{MeV}, \\ B(^{16}\mathrm{O}) &= B(^{12}\mathrm{C}) + B(\alpha) + 7.16\ \mathrm{MeV}, \\ B(^{20}\mathrm{Ne}) &= B(^{16}\mathrm{O}) + B(\alpha) + 4.73\ \mathrm{MeV}, \\ B(^{24}\mathrm{Mg}) &= B(^{20}\mathrm{Ne}) + B(\alpha) + 9.32\ \mathrm{MeV}. \end{aligned} \tag{2}$$

IX. SUMMARY AND CONCLUSION

Within an α-particle model approach the energies of the ^{12}C,^{16}O,^{20}Ne,^{24}Mg, and ^{32}S nuclei have been calculated assuming different α-molecule shapes: linear chain, triangle, square, tetrahedron, pentagon, trigonal bipyramid, square pyramid, hexagon, octahedron, octagon, and cube. Within a macroscopic mean-field approach the potential barriers governing the entrance and decay channels of these nuclei via α emission or absorption as well as more symmetric binary and ternary reactions have also been compared.

The rms radii of the prolate chains differ from the experimental rms radii of the ground states. The binding energies of the three-dimensional shapes at the contact point are higher than the binding energies of the planar configurations. The core $+\alpha$ cluster configuration leads always to the lowest potential barrier. The binding energies of these $4n$ nuclei can be determined within the sum of the binding energy of n α plus the number of bonds multiplied by 2.4 MeV or by the sum of the binding energies of one α and one of the daughter nuclei plus the Coulomb energy and the proximity energy between the two fragments. Further experimental studies are highly desirable to better know the shape of these nuclei and the validity and limit of the α-particle molecule model.

[1] J. A. Wheeler, Phys. Rev. **52**, 1083 (1937).
[2] L. R. Hafstad and E. Teller, Phys. Rev. **54**, 681 (1938).
[3] J. Zhang, W. D. M. Rae, and A. C. Merchant, Nucl. Phys. A **575**, 61 (1994).
[4] D. M. Brink, J. Phys.: Conf. Ser. **111**, 012001 (2008).
[5] H. Horiuchi, in *Cluster in Nuclei*, edited by C. Beck, Lecture Notes in Physics 848 (Springer-Verlag, Berlin, 2010), Vol. 1, p. 57.
[6] W. von Oertzen, M. Freer, and Y. Kanada-En'yo, Phys. Rep. **432**, 43 (2006).
[7] E. Epelbaum, H. Krebs, T. A. Lähde, D. Lee, Ulf-G. Meißner, and G. Rupak, Phys. Rev. Lett. **112**, 102501 (2014).
[8] R. Bijker and F. Iachello, Phys. Rev. Lett. **112**, 152501 (2014).
[9] T. Ichikawa, J. A. Maruhn, N. Itagaki, and S. Ohkubo, Phys. Rev. Lett. **107**, 112501 (2011).
[10] W. B. He, Y. G. Ma, X. G. Cao, X. Z. Cai, and G. Q. Zhang, Phys. Rev. Lett. **113**, 032506 (2014).
[11] T. Suhara, Y. Funaki, B. Zhou, H. Horiuchi, and A. Tohsaki, Phys. Rev. Lett. **112**, 062501 (2014).
[12] Y. Funaki, H. Horiuchi, W. von Oertzen, G. Röpke, P. Schuck, A. Tohsaki, and T. Yamada, Phys. Rev. C **80**, 064326 (2009).
[13] T. Ichikawa, J. A. Maruhn, N. Itagaki, K. Matsuyanagi, P.-G. Reinhard, and S. Ohkubo, Phys. Rev. Lett. **109**, 232503 (2012).
[14] D. J. Marin-Lambarri, R. Bijker, M. Freer, M. Gai, T. Kokalova, D. J. Parker, and C. Wheldon, Phys. Rev. Lett. **113**, 012502 (2014).
[15] M. Itoh, S. Ando, T. Aoki, H. Arikawa, S. Ezure, K. Harada, T. Hayamizu, T. Inoue, T. Ishikawa, K. Kato, H. Kawamura, Y. Sakemi, and A. Uchiyama, Phys. Rev. Lett. **113**, 102501 (2014).
[16] B. Buck, C. B. Dover, and J. P. Vary, Phys. Rev. C **11**, 1803 (1975).
[17] P. Chevallier, F. Scheibling, G. Goldring, I. Plesser, and M. W. Sachs, Phys. Rev. **160**, 827 (1967).
[18] M. Freer, M. P. Nicoli, S. M. Singer, C. A. Bremner, S. P. G. Chappell, W. D. M. Rae, I. Boztosun, B. R. Fulton, D. L. Watson, B. J. Greenhalgh, G. K. Dillon, R. L. Cowin, and D. C. Weisser, Phys. Rev. C **70**, 064311 (2004).
[19] A. H. Wuosmaa, R. R. Betts, B. B. Back, M. Freer, B. G. Glagola, Th. Happ, D. J. Henderson, P. Wilt, and I. G. Bearden, Phys. Rev. Lett. **68**, 1295 (1992).
[20] W. Broniowski and E. Ruiz Arriola, Phys. Rev. Lett. **112**, 112501 (2014).
[21] A. Astier, P. Petkov, M.-G. Porquet, D. S. Delion, and P. Schuck, Phys. Rev. Lett. **104**, 042701 (2010).
[22] G. Royer, A. Escudie, and B. Sublard, Phys. Rev. C **90**, 024607 (2014).
[23] W. von Oertzen, B. Gebauer, G. Efimov, V. Zherebchevsky, Tz. Kokalova, S. Thummerer, Ch. Schulz, H. G. Bohlen, D. Kamanin, C. Beck, D. Curien, P. Papka, M. Rousseau, G. Royer, and G. de Angelis, Eur. Phys. J. A **36**, 279 (2008).
[24] G. Royer and F. Haddad, J. Phys. G: Nucl. Part. Phys. **20**, L131 (1994).
[25] G. Royer and B. Remaud, Nucl. Phys. A **444**, 477 (1985).
[26] G. Royer, J. Phys. G **12**, 623 (1986).
[27] G. Royer and J. Gaudillot, Phys. Rev. C **84**, 044602 (2011).

[28] G. Royer, M. Jaffré, and D. Moreau, Phys. Rev. C **86**, 044326 (2012).
[29] G. Royer, J. Phys. G: Nucl. Part. Phys. **26**, 1149 (2000).
[30] G. Royer and R. Moustabchir, Nucl. Phys. A **683**, 182 (2001).
[31] Y. Kanada-En'yo, Phys. Rev. Lett. **81**, 5291 (1998).
[32] Y. Kanada-En'yo, Prog. Theor. Phys. **117**, 655 (2007).
[33] M. Chernykh, H. Feldmeier, T. Neff, P. von Neumann-Cosel, and A. Richter, Phys. Rev. Lett. **98**, 032501 (2007).
[34] E. Epelbaum, H. Krebs, T. A. Lähde, D. Lee, and Ulf-G. Meißner, Phys. Rev. Lett. **109**, 252501 (2012).
[35] V. Bradnova *et al.*, Nucl. Phys. A **734**, E92 (2004).